Electronic Properties of Fully Strained La$_{1-x}$Sr$_x$MnO$_3$ Thin Films Grown by Molecular Beam Epitaxy (0.15 ≤ x ≤ 0.45)

Sandeep Kumar Chaluvadi,* Vincent Polewczyk, Aleksandr Yu Petrov, Giovanni Vinai, Luca Braglia, Jose Manuel Diez, Victor Pierron, Paolo Perna, Laurence Mechin, Piero Torelli, and Pasquale Orgiani*

Read Online

ACCESS | Metrics & More | Article Recommendations | Supporting Information

ABSTRACT: The structural, electronic, and magnetic properties of Sr-hole-doped epitaxial La$_{1-x}$Sr$_x$MnO$_3$ (0.15 ≤ x ≤ 0.45) thin films deposited using the molecular beam epitaxy technique on 4° vicinal STO (001) substrates are probed by the combination of X-ray diffraction and various synchrotron-based spectroscopy techniques. The structural characterizations evidence a significant shift in the LSMO (002) peak to the higher diffraction angles owing to the increase in Sr doping concentrations in thin films. The nature of the LSMO Mn mixed-valence state was estimated from X-ray photoemission spectroscopy together with the relative changes in the Mn L$_{2,3}$ edges observed in X-ray absorption spectroscopy (XAS), both strongly affected by doping. CTM4XAS simulations at the XAS Mn L$_{2,3}$ edges reveal the combination of epitaxial strain, and different MnO$_6$ crystal field splitting give rise to a peak at ∼641 eV. The observed changes in the occupancy of the e$_g$ and the t$_{2g}$ orbitals as well as their binding energy positions toward the Fermi level with hole doping are discussed. The room-temperature magnetic properties were probed at the end by circular dichroism.
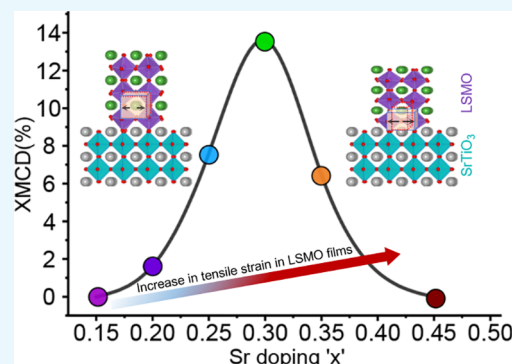
1. INTRODUCTION

Strongly correlated functional oxide perovskites have been known for their myriad properties such as two-dimensional electron gas, superconductivity, colossal magnetoresistance, half-metallicity, ferroelectricity, catalysis,[1−6] and so forth. Among the various known perovskites, La$_{1-x}$Sr$_x$MnO$_3$ (LSMO) with optimal doping has attracted the research community owing to room-temperature ferromagnetic metal (FM) and large spin-polarization.[5,7,8] This compound exhibits a rich electronic and magnetic phase diagram by tuning the hole-dopant Sr "x".[9,10] For instance, the parent compounds LaMnO$_3$ (x = 0) (Mn electronic configuration is 3d^4: t$_{2g}^3$e$_g^1$) and SrMnO$_3$ (x = 1) (3d^3: t$_{2g}^3$e$_g^0$) show antiferromagnetic (AFM) (A-type and G-type, respectively) and insulating (I) properties.[11,12] By considering the charge neutrality, substituting La by divalent Sr in parent LaMnO$_3$, the compound exhibits Mn mixed-valence states (Mn^{4+} and Mn^{3+}: 3d^3 and 3d^4). The Mn 3d electronic band-filling percentage in the t$_{2g}$ (xy, yz, zx) and e$_g$(x^2 − y^2, 3z^2 − r^2) orbitals differs with hole doping, influencing the macroscopic electronic and magnetic properties of the system. Furthermore, the structural distortion due to the Jahn−Teller (JT) effect adds an additional degree of freedom for electrons in selecting the preferential orbital occupancy.

For low doping (x < 0.17), an A-type AFM-I is observed.[12] In the doping regime 0.17 < x < 0.6, an FM behavior is favored, with the highest observable Curie temperature T$_c$ ≈ 350 K for the optimal doping x ≈ 0.33.[13] Due to large Hund's coupling and to the increase in the Mn−O−Mn bond angle, the probability of hopping electrons between Mn ions via O 2p orbitals enhances the double-exchange (DE) mechanism, giving rise to FM and metallic nature.[14−16] For doping levels x > 0.6, a charge-ordered AFM-I state is favored due to the suppression of DE. Distinctly from bulk and in addition to JT distortions, epitaxial strain imposed by the substrate in thin films adds additional constraints in selecting the orbital filling in the e$_g$ states, that is, tensile (compressive) strain that favors the in-plane (out-of-plane) x^2 − y^2 (3z^2 − r^2) orbitals.[17,18]

Although several studies have been performed on manganites, for instance, Hishida et al.[19] investigated the relationship between the valence-band X-ray photoelectron spectroscopy (XPS) spectral weights to the electrical conductivity of the entire Sr doping series of the polycrystalline La$_{1-x}$Sr$_x$MnO$_3$ samples, whereas Horiba et al.[20] studied the loss of spectral weight at the Fermi level and subsequent increase in the shoulder of the O 1s X-ray absorption spectroscopy (XAS) spectra and suggested pseudo-gap
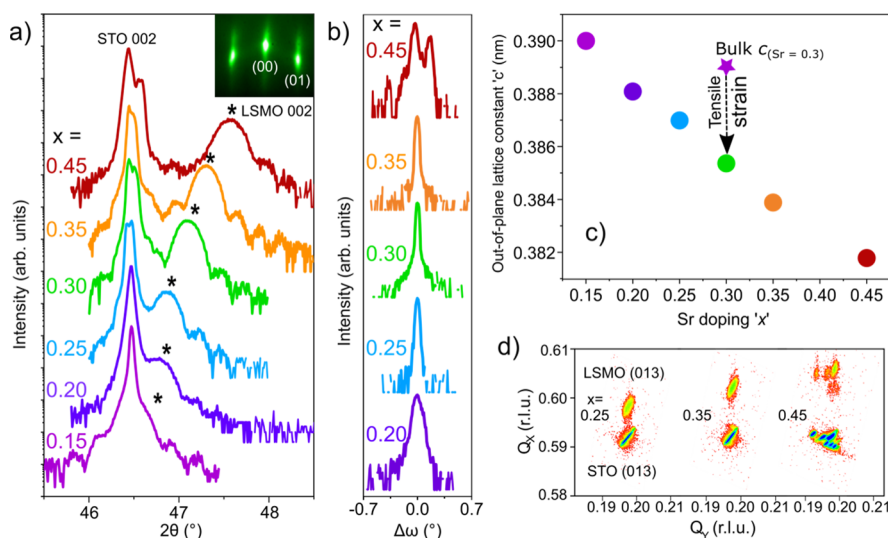
Figure 1. (a) $\theta-2\theta$ out-of-plane symmetrical XRD and the inset shows the RHEED pattern of the film, (b) ω-scan rocking curves measured along vicinal miscut (010) directions, (c) evolution of out-of-plane lattice parameter "c", and (d) asymmetrical RSM of LSMO thin films for various Sr doping. The star in panel (c) indicates the bulk lattice parameter of LSMO with Sr doping concentration $x = 0.3$.

formation with an increase in Sr doping in PLD-grown $La_{1-x}Sr_xMnO_3$ films. However, discrepancies between the expected ferromagnetic and the actual paramagnetic insulating behaviors of LSMO[21] as a function of doping (e.g., in Horiba et al.,[20] only Sr $\approx$ 0.3 and 0.4 doping levels do show an FM behavior at room temperature) often question possible oxygen vacancies[22] as well as the La/Sr/Mn stoichiometry.[21,23−25] Hence, there is a need to investigate in-detail a systematic study of Sr-doped $La_{1-x}Sr_xMnO_3$ films by careful tuning of the La/Sr cation ratio using the powerful molecular beam epitaxy (MBE) technique and by fixing the thickness realizing how the physical properties in thin films are affected with respect to the epitaxial strain imposed by the underlying substrate.[26]

Here, various Sr-doped ($0.15 \leq x \leq 0.45$) epitaxial LSMO thin films of thickness 120 unit cells (uc's) are deposited on 4° vicinal STO (001) substrates using the shutter MBE technique. The choice of vicinal substrates is due to induced uniaxial magnetic anisotropy with the easy axis parallel to the step edge direction being necessary for the design and development of anisotropic magnetoresistance sensors.[27,28] The structural, chemical, electronic, and magnetic properties are probed by means of X-ray diffraction (XRD), XPS, XAS, and X-ray magnetic circular dichroism (XMCD) spectroscopy techniques. XRD reveals the increase in tensile strain with an increase in doping "x", whereas XPS and XAS confirm the mixed-valence state of Mn ions. Valence band (Vb) spectra show substantial changes in the e_g, t_{2g} orbital occupancy, and changes in the ferromagnetic order are observed by XMCD. Finally, the common attribution of the intense peak in XAS spectra at ~641 eV is found to be due to the combination of epitaxial strain and different MnO_6 crystal field splitting by CTM4XAS simulations instead of the formation of Mn^{2+} ions.

2. EXPERIMENTAL DETAILS

Sr dopant concentration-dependent epitaxial LSMO (001) thin films of thickness 120 uc's were coherently grown on to (001)-oriented 4°tw vicinal $SrTiO_3$ (STO) substrates using the shutter layer-by-layer MBE technique.[29] The as-received substrates were sonicated in acetone and ethanol solutions and subsequently dried under a N_2 atmosphere prior to be inserted into the MBE deposition system. The deposition of the films was made by maintaining the substrate temperature of about 720 °C and the ozone background pressure was kept at 2×10^{-6} mbar. After deposition, films were cooled down to room temperature under the same deposition pressure. By taking advantage of the *in situ* reflection high energy electron diffraction (RHEED) technique, thickness and Sr doping concentrations in the films were controlled. The growth rate of the films was about 1 uc per minute.

The structural characterization of all films was performed by monitoring both *in situ* RHEED oscillations and *ex situ* PANalytical X'Pert Pro XRD using monochromatic Cu Kα_1 radiation (λ = 1.54056 Å) in the Bragg−Brentano configuration. Rocking curves of the films were measured using high-resolution XRD with incident optics composed of double Ge(440) and diffracted optics composed of a 3-axis monochromator. The chemical composition and electronic properties of the films were characterized using linearly polarized soft X-ray synchrotron radiation techniques such as XPS and XAS spectroscopies at the APE-HE beamline at Elettra synchrotron.[30] The XAS measurements at the Mn $L_{2,3}$ edges were performed in the total electron yield (TEY) mode with a grazing angle of 45° with respect to the beam. The drain current of a reference mesh was measured simultaneously and independently from the sample for the alignment and normalization of the spectra. XMCD measurements were taken in circular polarization, by measuring the TEY signal at remanence after the application of an in-plane magnetic pulse of ±30 mT at each energy step. The magnitude of the applied magnetic field (±30 mT) is sufficient to saturate the sample, as it was observed from MOKE measurements (not presented here). The dichroic signal is calculated by considering the 75% degree of polarization and the 45° of angle incidence. Core-level and Vb XPS spectra were acquired using an Omicron E125 hemispherical analyzer with an incident photon excitation energy of 1000 and 470 eV, respectively.

3. RESULTS AND DISCUSSION

3.1. Structural Characterization. $\theta-2\theta$ out-of-plane XRD was performed on the films with different Sr doping
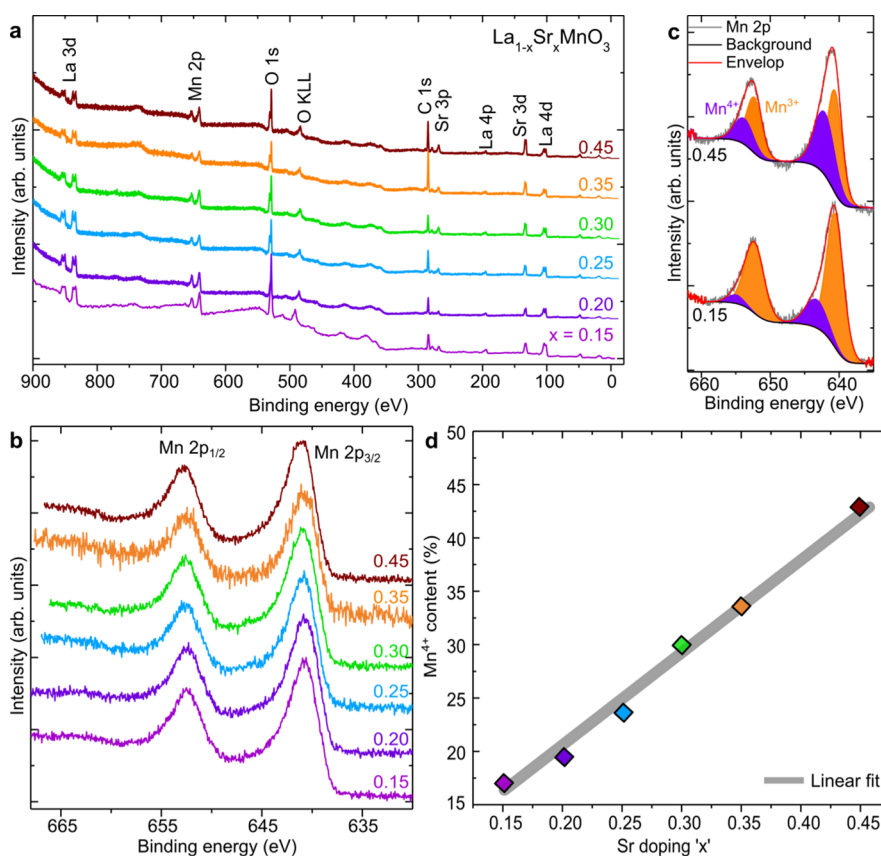
Figure 2. (a) XPS survey scan, (b) Mn 2p of $La_{1-x}Sr_xMnO_3$ thin films with different Sr doping concentrations x, (c) Mn 2p for 0.15 and 0.45 Sr with Mn^{3+} and Mn^{4+} peak-fitting components, and (d) Mn^{4+} content as a function of Sr doping. The measurements are performed with photon excitation energy $h\nu$ = 1000 eV.

contents by aligning the substrate vicinal miscut angle with respect to the incident X-ray beam. The films have grown epitaxially on the STO substrate, showing the (00*l*) orientation (Figure 1a), and all the films show detailed finite-size structural effects, indicating a very high crystalline quality of the films. In addition, we have observed that the LSMO (002) film peak position ("*" in Figure 1a) shifts toward higher diffraction angles with an increase in Sr doping. The out-of-plane lattice parameter "*c*" calculated from the (002) LSMO peak is reduced from 0.39 to 0.382 nm with an increase in Sr doping from 0.15 to 0.45. Figure 1c shows the evolution of the *c*-axis lattice parameter of LSMO films with various Sr doping. By substituting Sr by La in the parent compound $LaMnO_3$, the pseudocubic lattice parameter decreases from 0.3944 to 0.3805 nm for $LaMnO_3$ to $SrMnO_3$, respectively. As the films are grown on STO with the cubic lattice constant a = 0.3905 nm, the film experiences higher tensile strain and consequent reduction of the out-of-plane lattice constant "*c*" with an increase in Sr doping.[13,31] The estimated Poisson ratio for the films is ∼0.36 ± 0.02, which is a typical value for oxides and manganites.[32,33] The RHEED pattern shown in the inset of Figure 1a with well-defined sharp diffraction streaks corresponds to a long-range crystallinity order of the film.

In addition, the quality of the films and the misalignment of the LSMO cell with the substrate were verified through rocking curve analysis. The omega scan rocking curves were obtained at the (002) peaks of LSMO by aligning the X-ray beam along the vicinal directions. Figure 1b depicts the rocking curves of all the various Sr-doped LSMO films measured along the

miscut direction, showing a single sharp peak with full-width half maximum values in the range of 0.068 ± 0.02°. Such a value is similar to that of our STO substrates, indicating very high film crystallinity. Asymmetrical reciprocal space maps (RSMs) were obtained around the (013) Bragg reflections of both the LSMO film and STO substrate, as shown in Figure 1d. The scattering vectors Q_y of both film and substrate are vertically aligned for different Sr doping concentrations, confirming that the LSMO films are pseudomorphically grown on the STO substrate. Hence, the films are fully tensile-strained and the in-plane lattice constants "*a*" of the film match with those of the substrate.

3.2. X-ray Photoemission and Absorption Spectroscopy. To investigate the elemental composition and Mn oxidation states in LSMO films, XPS measurements are performed at the APE-HE beamline. Figure 2a shows the XPS survey scans of different Sr-doped LSMO thin films measured with linearly polarized photon excitation energy $h\nu$ = 1000 eV. The XPS survey scan reveals all the expected elements with features of La 3d, Mn 2p, O 1s, Sr 3d, and La 4d edges. As the films are measured *ex situ*, except the C 1s peak, no other traces of impurities are observed on the film surface.

The Mn 2p core-level spectra of various Sr-doped LSMO films in the binding energy range of 670−635 eV are shown in Figure 2b. All the Mn 2p spectra show similar features with spin−orbit doublets Mn $2p_{3/2}$ and Mn $2p_{1/2}$ located around ∼641 and ∼653 eV, respectively, and the spin−orbit splitting of ∼12 eV. A small bump located at ∼662 eV is a charge transfer satellite peak of Mn $2p_{1/2}$.[34] Since the films were
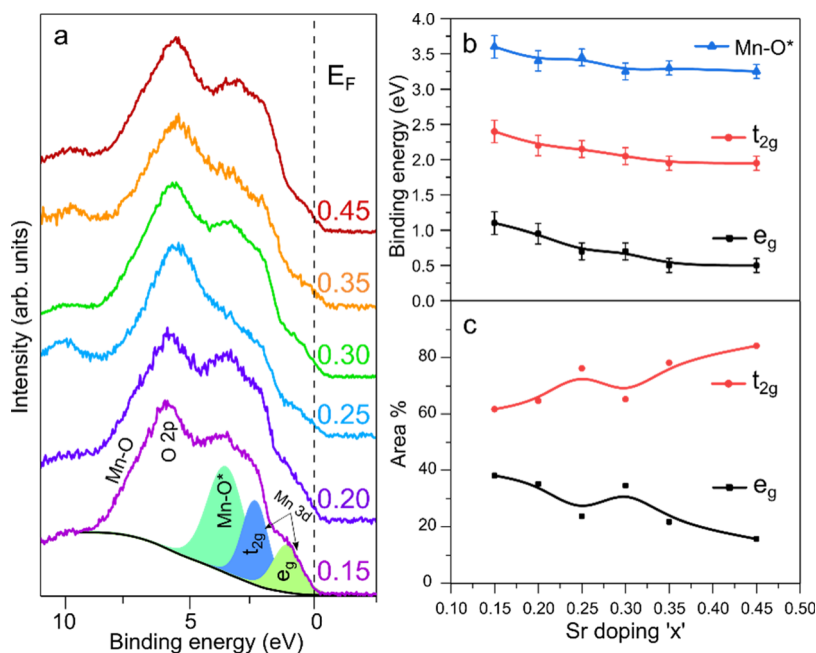
Figure 3. (a) XPS valence-band spectra (10−0 eV binding energy range) taken at the photon energy $h\nu$ of 470 eV, (b) binding energy peak positions of e_g, t_{2g}, and Mn−O* hybridization peaks, and (c) e_g and t_{2g} spectral weights for various Sr doping in films, respectively.

measured *ex situ*, the well-screened metallic peak at the lower binding energies is not visible, which otherwise is observed either on unexposed samples[35] or by hard X-ray photoemission.[19,36] In order to estimate the Mn valence state in the films, Mn 2p core-level spectra were fitted using mixed Gaussian-Lorentzian line shapes after subtracting the background intensity due to the presence of secondary electrons using the Shirley background. The comparison between the 0.15 and 0.45 Sr-doped LSMO films along with Mn^{3+} (orange shaded region) and Mn^{4+} (violet shaded region) fitting components is depicted in Figure 2c. By estimating the spectral weights of the Mn^{3+} and Mn^{4+} peaks, a systematic linear trend is found, that is, an increase in the percentage of Mn^{4+} content in correspondence to an increase in Sr-hole doping in the LSMO films, as shown in Figure 2d. Therefore, the MBE technique is advantageous in the fine tuning of doping concentrations, which is essential for the development of artificial multilayers and heterostructures.

Doping-induced subtle electronic changes in LSMO films are directly reflected in the XPS Vb spectra analysis, as presented in Figure 3. Figure 3a shows the Vb spectra in the binding energy range of 0−10 eV, taken at a photon energy of 470 eV for various Sr-doped LSMO films. The spectral assignments from the Fermi level E_F are designated to Mn 3d e_g (0.5−1 eV), Mn 3d t_{2g} (2−2.5 eV), and Mn 3d−O 2p hybridization (~3.5 and ~7.5 eV) and with an intense O 2p peak (~5.6 eV), respectively.[20,37−40] Hong et al.[41] demonstrated that in perovskite systems ($LaMnO_3$, $LaCoO_3$, etc.), the O 2p nonbonding states can straddle between two transition metal and oxygen (TM-O) hybridization states and are associated with the antibonding and bonding states. Therefore, the highly intense peak at the BE of ~5.6 eV is assigned to O 2p nonbonding states, whereas the strongly hybridized Mn 3d−O 2p peaks that are present at ~3.5 eV belong to the antibonding state and denoted as Mn−O* and the weak shoulder at the BE ≈ 7.5 eV belongs to the bonding states of Mn−O.

While O 2p nonbonding states and Mn−O* hybridization peaks are present almost at the same binding energies of ~5.6 and ~3.5 eV for all the Sr doping levels, interesting changes have been observed in the e_g and t_{2g} states. While the binding energy position of the e_g state for 0.15 Sr doping is located at ~1.1 eV, upon increasing the Sr doping concentration in the films, the e_g state tends to move closer to the E_F level, reaching ~0.5 eV for 0.45 Sr. Similar to the e_g state, the t_{2g} state-binding energy position also moves toward E_F, going from ~2.45 to ~1.9 eV for 0.15 to 0.45 Sr doping, as shown in Figure 3b. Subsequently, the spectral weights calculated under the e_g (t_{2g}) state reduces (enhances) with the increase in hole doping (Figure 3c), indicating the decrease (increase) in e_g band filling.[42] This results in an increase in the electron hopping parameter, thus enhancing the conductivity and favoring the ferromagnetic order with hole doping, as it will be discussed in the XMCD section.

The changes in the electronic structure induced by different Sr doping contents in LSMO films were then probed by XAS at Mn $L_{2,3}$ edges, as shown in Figure 4a. A reference signal acquired simultaneously with the spectra allowed us to correctly align the spectra in energy. As described in the introduction, the electronic configuration of the Mn 3d in a purely electron-doped (LMO) and hole-doped (SMO) system is $t_{2g}^3 e_g^1$ (Mn^{3+}) and $t_{2g}^3 e_g^0$ (Mn^{4+}), respectively, while the intermediate doping regime presents mixed Mn^{3+} and Mn^{4+} valence states. Therefore, the Mn XAS features will be sensitive to any changes in both doping concentrations. We therefore observed that by increasing the Sr doping level from 0.15 to 0.45, a shift of the main Mn L_3 edge of 0.48 eV takes place toward the higher photon energy.

To attribute the valence contributions of each spectrum, simulations were performed using CTM4XAS software, as seen in Figure 4b.[43] First, we have simulated XAS spectra for different Mn valence states (Mn^{2+}, Mn^{3+}, and Mn^{4+}). The ligand field multiplet theory, implemented in the CTM4XAS program, was adopted to simulate the theoretical Mn $L_{2,3}$ edge
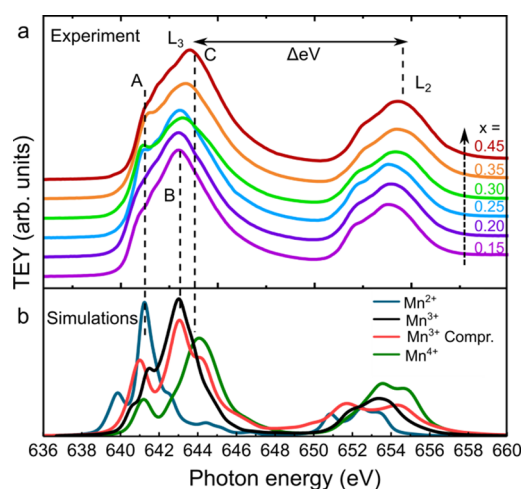
Figure 4. (a) Mn $L_{2,3}$ edge XAS spectra of 120 uc LSMO films with various Sr doping concentrations and (b) XAS Mn $L_{2,3}$ edges simulated for different valence states. Dashed vertical gray lines indicate the correspondence between experimental and simulated peaks for the different doping levels.

3.3. XMCD. In order to have a deeper understanding of the role of the Sr dopant on the changes in magnetic properties, XMCD measurements at the Mn $L_{2,3}$-edge were performed at room temperature, that is, 300 K. Figure 5 shows the XMCD

Figure 5. XMCD spectra at Mn $L_{2,3}$ edges for the various doping levels of $La_{1-x}Sr_xMnO_3$ thin films measured at room temperature (300 K). The inset shows the XMCD % at the L_3 edge as a function of Sr doping concentration.

spectra. The theoretical parameters are reported in Table S1. The hybridization of Mn with oxygen ligands was considered in the calculations by reducing the Slater integrals from their atomic values. The Mn^{3+} symmetry is considered to be D_{4h} (due to a Jahn−Teller distortion) and the Mn^{2+} and Mn^{4+} to be O_h.[44] The charge transfer parameters for Mn^{2+}, Mn^{3+}, and Mn^{4+} were selected from previous work on MnO, $LaMnO_3$, and MnO_2, respectively.[45−49] The crystal field parameters D_s and D_t (tetragonal parameters) for the Mn^{3+}, generated from the transition O_h to D_{4h} distortion,[50,51] were selected with the opposite sign that indicates an axial compression (compression of the octahedral/tensile strain) in LSMO sample growth on STO substrates. The relative concentration of Mn^{3+} and Mn^{4+} was chosen from the previous Mn quantification performed on the Mn 2p XPS fit. From 0.25 to 0.35 Sr concentration, we observed the rise of a sharp intense peak at 641 eV (A in Figure 4a). We proposed two hypotheses about this observation: (i) Mn^{2+} formation and (ii) an increase in the JT distortion in Mn^{3+}. The former is supported by the intense peak of the theoretical Mn^{2+} that is at around 641 eV, and moreover, there is a wide bibliography on the Mn^{2+} formation in an air-exposed LSMO system,[52] while the latter is supported by the previous XPS measurement in which the Mn^{2+} presence was not observed, in addition to the epitaxial strain in the film (Figure 1). For this reason, we proposed another Mn^{3+*}-simulated spectrum where the 10 Dq was increased to 2 eV: in this way, the final energy of d_z^2 orbitals increased and it describes a stronger compression of MnO_6 octahedra (Figure 4b). It is worth to note that the Mn^{3+*} has an intense peak at 641 eV as the Mn^{2+}. Hence, our simulations suggest that the epitaxial strain in the film leads to different crystal field splitting and would therefore attribute the peak present at ∼641 eV to an Mn^{3+} contribution instead of an Mn^{2+} one.

Finally, the energy splitting (Δ eV) between the L_2 and L_3 maximum peak intensity edges decreased from 10.8 eV for 0.15 Sr to 10.6 eV for 0.45 Sr doping. Such a similar energy difference trend was also observed previously in divalent Ca-doped manganite perovskite $Pr_{1-x}Ca_xMnO_3$ thin films and attributed the difference to the increase in the valence state of Mn.[53,54]
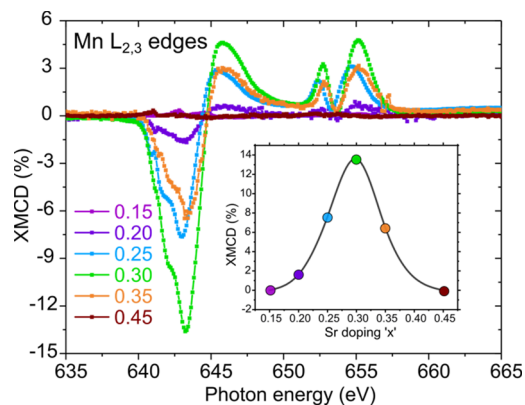
spectra of the sample series with Sr doping from 0.15 to 0.45. The inset of Figure 5 shows the maximum XMCD % that systematically increases with the increase in Sr content in films from 0.20 and reaches the maximum value of about 12−13% for 0.30 and then decreases. By considering the LSMO phase diagram,[55] the optimal doping regime (Sr ≈ 0.3) exhibits the highest ferromagnetic ordering, which is in good agreement with the XMCD results obtained here. The XMCD signal for the film grown with 0.15 and 0.45 Sr doping concentrations are almost flat, indicating a negligible FM order possibly due to the arising of the AFM one.

4. CONCLUSIONS

We have successfully deposited epitaxial LSMO thin films by fine-tuning of Sr doping (0.15 ≤ x ≤ 0.45) in films using the MBE technique and extensively studied their structural, chemical, electronic, and magnetic properties using XRD and different synchrotron-based spectroscopy techniques. For all Sr concentrations, films were fully strained with the underlying STO substrate, thus showing a linear decrease in the out-of-plane lattice parameter "c" with an increase in Sr-hole doping content. Valence-band XPS shows that the spectral weight area of e_g (t_{2g}) decreases (increases) and the peak positions also move closer to E_F as Sr-hole doping increases in films. The electronic states measured by XAS at Mn $L_{2,3}$ edges also show significant shift toward higher photon energy with the increase in Sr doping levels. The differences in energy splitting between Mn $L_{2,3}$ edges, that is, Δ eV from 10.8 to 10.6 eV correspond to the changes in the Mn valence state with Sr-hole doping. The additional shoulder peak in XAS present at ∼641 eV for the intermediate doping levels (0.25−0.35) was attributed to the epitaxial strain and crystal field splitting of the MnO_6 octahedral network. This systematic study will serve as a template for the studies of various hole-doped manganites/perovskite systems.

■ ASSOCIATED CONTENT

Ⓢ Supporting Information

The Supporting Information is available free of charge at https://pubs.acs.org/doi/10.1021/acsomega.1c06529.

Theoretical parameters used for the simulations of XAS Mn $L_{2,3}$ edges in CTM4XAS software (PDF)

■ AUTHOR INFORMATION

Corresponding Authors

Sandeep Kumar Chaluvadi − *Istituto Officina dei Materiali (IOM)−CNR, Laboratorio TASC, I-34149 Trieste, Italy;* ⓞ orcid.org/0000-0002-3689-3336; Email: chaluvadi@iom.cnr.it

Pasquale Orgiani − *Istituto Officina dei Materiali (IOM)−CNR, Laboratorio TASC, I-34149 Trieste, Italy;* ⓞ orcid.org/0000-0002-1082-9651; Email: pasquale.orgiani@cnr.it

Authors

Vincent Polewczyk − *Istituto Officina dei Materiali (IOM)−CNR, Laboratorio TASC, I-34149 Trieste, Italy*

Aleksandr Yu Petrov − *Istituto Officina dei Materiali (IOM)−CNR, Laboratorio TASC, I-34149 Trieste, Italy*

Giovanni Vinai − *Istituto Officina dei Materiali (IOM)−CNR, Laboratorio TASC, I-34149 Trieste, Italy;* ⓞ orcid.org/0000-0003-4882-663X

Luca Braglia − *Istituto Officina dei Materiali (IOM)−CNR, Laboratorio TASC, I-34149 Trieste, Italy;* ⓞ orcid.org/0000-0003-0796-3670

Jose Manuel Diez − *IMDEA-Nanociencia, 28049 Madrid, Spain*

Victor Pierron − *Normandie Univ, UNICAEN, ENSICAEN, CNRS, GREYC (UMR 6072), 14000 Caen, France*

Paolo Perna − *IMDEA-Nanociencia, 28049 Madrid, Spain;* ⓞ orcid.org/0000-0001-8537-4834

Laurence Mechin − *Normandie Univ, UNICAEN, ENSICAEN, CNRS, GREYC (UMR 6072), 14000 Caen, France;* ⓞ orcid.org/0000-0002-6350-1801

Piero Torelli − *Istituto Officina dei Materiali (IOM)−CNR, Laboratorio TASC, I-34149 Trieste, Italy*

Complete contact information is available at:
https://pubs.acs.org/10.1021/acsomega.1c06529

Notes

The authors declare no competing financial interest.

■ ACKNOWLEDGMENTS

■ REFERENCES

(1) Ohtomo, A.; Hwang, H. Y. A high-mobility electron gas at the LaAlO3/SrTiO3 heterointerface. *Nature* **2004**, *427*, 423.

(2) Dagotto, E. Complexity in Strongly Correlated Electronic Systems. *Science* **2005**, *309*, 257−262.

(3) Jin, S.; Tiefel, T. H.; McCormack, M.; Fastnacht, R. A.; Ramesh, R.; Chen, L. H. Thousandfold Change in Resistivity in Magnetoresistive La-Ca-Mn-O Films. *Science* **1994**, *264*, 413−415.

(4) Rondinelli, J. M.; Spaldin, N. A. Structure and Properties of Functional Oxide Thin Films: Insights from Electronic-Structure Calculations. *Adv. Mater.* **2011**, *23*, 3363−3381.

(5) Tokura, Y.; Tomioka, Y. Colossal Magnetoresistive Manganites. *J. Magn. Magn. Mater.* **1999**, *200*, 1−23.

(6) Catalan, G.; Scott, J. F. Physics and Applications of Bismuth Ferrite. *Adv. Mater.* **2009**, *21*, 2463−2485.

(7) Prellier, W.; Lecoeur, P.; Mercey, B. Colossal-magnetoresistive manganite thin films. *J. Phys.: Condens. Matter* **2001**, *13*, R915−R944.

(8) Chaluvadi, S. K.; Ajejas, F.; Orgiani, P.; Rousseau, O.; Vinai, G.; Petrov, A. Y.; Torelli, P.; Pautrat, A.; Camarero, J.; Perna, P.; Mechin, L. Room temperature biaxial magnetic anisotropy in La0.67Sr0.33MnO3 thin films on SrTiO3 buffered MgO (001) substrates for spintronic applications. *Appl. Phys. Lett.* **2018**, *113*, 052403.

(9) Fujishiro, H.; Fukase, T.; Ikebe, M. Charge Ordering and Sound Velocity Anomaly in La1-XSrXMnO3(X≥0.5). *J. Phys. Soc. Jpn.* **1998**, *67*, 2582−2585.

(10) Majumdar, S.; Dijken, S. v. Pulsed laser deposition of La1−xSrxMnO3: thin-film properties and spintronic applications. *J. Phys. D Appl. Phys.* **2014**, *47*, 034010.

(11) Adamo, C.; Ke, X.; Schiffer, P.; Soukiassian, A.; Warusawithana, M.; Maritato, L.; Schlom, D. G. Electrical and magnetic properties of (SrMnO3)n/(LaMnO3)2n superlattices. *Appl. Phys. Lett.* **2008**, *92*, 112508.

(12) Kawano, H.; Kajimoto, R.; Kubota, M.; Yoshizawa, H. Canted antiferromagnetism in an insulating lightly dopedLa1−xSrxMnO3-withx≤0.17. *Phys. Rev. B: Condens. Matter Mater. Phys.* **1996**, *53*, 2202−2205.

(13) Urushibara, A.; Moritomo, Y.; Arima, T.; Asamitsu, A.; Kido, G.; Tokura, Y. Insulator-metal transition and giant magnetoresistance inLa1−xSrxMnO3. *Phys. Rev. B: Condens. Matter Mater. Phys.* **1995**, *51*, 14103−14109.

(14) Zener, C. Interaction between thed-Shells in the Transition Metals. II. Ferromagnetic Compounds of Manganese with Perovskite Structure. *Phys. Rev.* **1951**, *82*, 403−405.

(15) Zener, C. Interaction Between thedShells in the Transition Metals. *Phys. Rev.* **1951**, *81*, 440−444.

(16) Chaluvadi, S. K.; Ajejas, F.; Orgiani, P.; Lebargy, S.; Minj, A.; Flament, S.; Camarero, J.; Perna, P.; Méchin, L. Epitaxial strain and thickness dependent structural, electrical and magnetic properties of La0.67Sr0.33MnO3 films. *J. Phys. D Appl. Phys.* **2020**, *53*, 375005.

(17) Pesquera, D.; Herranz, G.; Barla, A.; Pellegrin, E.; Bondino, F.; Magnano, E.; Sánchez, F.; Fontcuberta, J. Surface Symmetry-Breaking and Strain Effects on Orbital Occupancy in Transition Metal Perovskite Epitaxial Films. *Nat. Commun.* **2012**, *3*, 1189.

(18) Bigi, C.; Kumar Chaluvadi, S.; Galdi, A.; Maritato, L.; Aruta, C.; Ciancio, R.; Fujii, J.; Gobaut, B.; Torelli, P.; Vobornik, I.; Panaccione, G.; Rossi, G.; Orgiani, P. Predominance of Z2-Orbitals at the Surface of Both Hole- and Electron-Doped Manganites. *J. Electron Spectrosc. Relat. Phenom.* **2020**, *245*, 147016.

(19) Hishida, T.; Ohbayashi, K.; Kobata, M.; Ikenaga, E.; Sugiyama, T.; Kobayashi, K.; Okawa, M.; Saitoh, T. Empirical relationship between x-ray photoemission spectra and electrical conductivity in a colossal magnetoresistive manganite La1−xSrxMnO3. *J. Appl. Phys.* **2013**, *113*, 233702.

(20) Horiba, K.; Chikamatsu, A.; Kumigashira, H.; Oshima, M.; Nakagawa, N.; Lippmaa, M.; Ono, K.; Kawasaki, M.; Koinuma, H. In vacuophotoemission study of atomically controlledLa1−xSrxMnO3-thin films: Composition dependence of the electronic structure. *Phys. Rev. B: Condens. Matter Mater. Phys.* **2005**, *71*, 155420.

(21) Liao, Z.; Zhang, J. Metal-to-Insulator Transition in Ultrathin Manganite Heterostructures. *Appl. Sci.* **2019**, *9*, 144.

(22) Orgiani, P.; Petrov, A. Y.; Ciancio, R.; Galdi, A.; Maritato, L.; Davidson, B. A. Evidence of Direct Correlation between Out-of-Plane

Lattice Parameter and Metal-Insulator Transition Temperature in Oxygen-Depleted Manganite Thin Films. *Appl. Phys. Lett.* **2012**, *100*, 042404.

(23) Ciancio, R.; Carlino, E.; Aruta, C.; MacCariello, D.; Granozio, F. M.; Scotti Di Uccio, U. Nanostructure of buried interface layers in TiO2anatase thin films grown on LaAlO3and SrTiO3substrates. *Nanoscale* **2011**, *4*, 91−94.

(24) Gömann, K.; Borchardt, G.; Schulz, M.; Gömann, A.; Maus-Friedrichs, W.; Lesage, B.; Kaïtasov, O.; Hoffmann-Eifert, S.; Schneller, T. Sr diffusion in undoped and La-doped SrTiO3single crystals under oxidizing conditions. *Phys. Chem. Chem. Phys.* **2005**, *7*, 2053−2060.

(25) Chou, H.; Hsu, S. G.; Lin, C. B.; Wu, C. B. Interdiffusion Effect on Strained La0.8Ba0.2MnO3 Thin Films by off-Axis Sputtering on SrTiO3 (100) Substrates. *Appl. Phys. Lett.* **2007**, *90*, 062501.

(26) Petrov, A. Y.; Torrelles, X.; Verna, A.; Xu, H.; Cossaro, A.; Pedio, M.; Garcia-Barriocanal, J.; Castro, G. R.; Davidson, B. A. Surface Octahedral Distortions and Atomic Design of Perovskite Interfaces. *Adv. Mater.* **2013**, *25*, 4043−4048.

(27) Perna, P.; Maccariello, D.; Ajejas, F.; Guerrero, R.; Méchin, L.; Flament, S.; Santamaria, J.; Miranda, R.; Camarero, J. Engineering Large Anisotropic Magnetoresistance in La0.7 Sr0.3 MnO3 Films at Room Temperature. *Adv. Funct. Mater.* **2017**, *27*, 1700664.

(28) Rousseau, O.; Flament, S.; Guillet, B.; Sing, M. L. C.; Méchin, L. Magnetic Sensors Based on AMR Effect in LSMO Thin Films. *Proceedings* **2017**, *1*, 635.

(29) Vinai, G.; Motti, F.; Petrov, A. Y.; Polewczyk, V.; Bonanni, V.; Edla, R.; Gobaut, B.; Fujii, J.; Suran, F.; Benedetti, D.; Salvador, F.; Fondacaro, A.; Rossi, G.; Panaccione, G.; Davidson, B. A.; Torelli, P. An Integrated Ultra-High Vacuum Apparatus for Growth and in Situ Characterization of Complex Materials. *Rev. Sci. Instrum.* **2020**, *91*, 085109.

(30) Panaccione, G.; Vobornik, I.; Fujii, J.; Krizmancic, D.; Annese, E.; Giovanelli, L.; Maccherozzi, F.; Salvador, F.; De Luisa, A.; Benedetti, D.; Gruden, A.; Bertoch, P.; Polack, F.; Cocco, D.; Sostero, G.; Diviacco, B.; Hochstrasser, M.; Maier, U.; Pescia, D.; Back, C. H.; Greber, T.; Osterwalder, J.; Galaktionov, M.; Sancrotti, M.; Rossi, G. Advanced Photoelectric Effect Experiment Beamline at Elettra: A Surface Science Laboratory Coupled with Synchrotron Radiation. *Rev. Sci. Instrum.* **2009**, *80*, 043105.

(31) Nardi, A.; Bigi, C.; Kumar Chaluvadi, S.; Ciancio, R.; Fujii, J.; Vobornik, I.; Panaccione, G.; Rossi, G.; Orgiani, P. Analysis of Metal-Insulator Crossover in Strained SrRuO3 Thin Films by X-Ray Photoelectron Spectroscopy. *Coatings* **2020**, *10*, 780.

(32) Fehringer, G.; Janes, S.; Wildersohn, M.; Clasen, R. Proton-Conducting Ceramics as Electrode/Electrolyte-Materials for SOFCs: Preparation, Mechanical and Thermal-Mechanical Properties of Thermal Sprayed Coatings, Material Combination and Stacks. *J. Eur. Ceram. Soc.* **2004**, *24*, 705−715.

(33) Adamo, C.; Ke, X.; Wang, H. Q.; Xin, H. L.; Heeg, T.; Hawley, M. E.; Zander, W.; Schubert, J.; Schiffer, P.; Muller, D. A.; Maritato, L.; Schlom, D. G. Effect of Biaxial Strain on the Electrical and Magnetic Properties of (001) La0.7Sr0.3MnO3 Thin Films. *Appl. Phys. Lett.* **2009**, *95*, 112504.

(34) Saitoh, T.; Bocquet, A. E.; Mizokawa, T.; Namatame, H.; Fujimori, A.; Abbate, M.; Takeda, Y.; Takano, M. Electronic structure ofLa1−xSrxMnO3studied by photoemission and x-ray-absorption spectroscopy. *Phys. Rev. B: Condens. Matter Mater. Phys.* **1995**, *51*, 13942−13951.

(35) Hishida, T.; Ohbayashi, K.; Saitoh, T. Hidden relationship between the electrical conductivity and the Mn 2p core-level photoemission spectra in La1−xSrxMnO3. *J. Appl. Phys.* **2013**, *113*, 043710.

(36) Horiba, K.; Taguchi, M.; Chainani, A.; Takata, Y.; Ikenaga, E.; Miwa, D.; Nishino, Y.; Tamasaku, K.; Awaji, M.; Takeuchi, A.; Yabashi, M.; Namatame, H.; Taniguchi, M.; Kumigashira, H.; Oshima, M.; Lippmaa, M.; Kawasaki, M.; Koinuma, H.; Kobayashi, K.; Ishikawa, T.; Shin, S. Nature of the Well Screened State in Hard X-Ray Mn2pCore-Level Photoemission Measurements ofLa1−xSrxMnO3Films. *Phys. Rev. Lett.* **2004**, *93*, 236401.

(37) Schlueter, C.; Orgiani, P.; Lee, T.-L.; Petrov, A. Y.; Galdi, A.; Davidson, B. A.; Zegenhagen, J.; Aruta, C. Evidence of electronic band redistribution in La0.65Sr0.35MnO3−δby hard x-ray photoelectron spectroscopy. *Phys. Rev. B: Condens. Matter Mater. Phys.* **2012**, *86*, 155102.

(38) Picozzi, S.; Ma, C.; Yang, Z.; Bertacco, R.; Cantoni, M.; Cattoni, A.; Petti, D.; Brivio, S.; Ciccacci, F. Oxygen vacancies and induced changes in the electronic and magnetic structures ofLa0.66Sr0.33MnO3: A combinedab initioand photoemission study. *Phys. Rev. B: Condens. Matter Mater. Phys.* **2007**, *75*, 094418.

(39) Bertacco, R.; Tagliaferri, A.; Riva, M.; Signorini, L.; Cantoni, M.; Cattoni, A.; Ciccacci, F.; Davidson, B. A.; Maccherozzi, F.; Vobornik, I.; Panaccione, G. Surface electronic and magnetic properties ofLa2/3Sr1/3MnO3thin films with extended metallicity above the Curie temperature. *Phys. Rev. B: Condens. Matter Mater. Phys.* **2008**, *78*, 035448.

(40) Schlueter, C.; Aruta, C.; Yang, N.; Tebano, A.; Di Castro, D.; Balestrino, G.; Lee, T. L. Tuning Electronic Reconstructions at the Cuprate-Manganite Interface. *Phys. Rev. Mater.* **2019**, *3*, 094406.

(41) Hong, W. T.; Stoerzinger, K. A.; Moritz, B.; Devereaux, T. P.; Yang, W.; Shao-Horn, Y. Probing LaMO3 Metal and Oxygen Partial Density of States Using X-Ray Emission, Absorption, and Photoelectron Spectroscopy. *J. Phys. Chem. C* **2015**, *119*, 2063−2072.

(42) Wadati, H.; Kobayashi, D.; Kumigashira, H.; Okazaki, K.; Mizokawa, T.; Fujimori, A.; Horiba, K.; Oshima, M.; Hamada, N.; Lippmaa, M.; Kawasaki, M.; Koinuma, H. Hole-doping-induced changes in the electronic structure ofLa1−xSrxFeO3: Soft x-ray photoemission and absorption study of epitaxial thin films. *Phys. Rev. B: Condens. Matter Mater. Phys.* **2005**, *71*, 035108.

(43) Stavitski, E.; de Groot, F. M. F. The CTM4XAS Program for EELS and XAS Spectral Shape Analysis of Transition Metal L Edges. *Micron* **2010**, *41*, 687−694.

(44) Cuartero, V.; Lafuerza, S.; Rovezzi, M.; García, J.; Blasco, J.; Subías, G.; Jiménez, E. X-ray absorption and emission spectroscopy study of Mn and Co valence and spin states inTbMn1−xCoxO3. *Phys. Rev. B* **2016**, *94*, 155117.

(45) Zhong, X.; Oubla, M. h.; Wang, X.; Huang, Y.; Zeng, H.; Wang, S.; Liu, K.; Zhou, J.; He, L.; Zhong, H.; Alonso-Vante, N.; Wang, C.-W.; Wu, W.-B.; Lin, H.-J.; Chen, C.-T.; Hu, Z.; Huang, Y.; Ma, J. Boosting Oxygen Reduction Activity and Enhancing Stability through Structural Transformation of Layered Lithium Manganese Oxide. *Nat. Commun.* **2021**, *12*, 3136.

(46) De Groot, F. M. F. X-Ray Absorption and Dichroism of Transition Metals and Their Compounds. *J. Electron Spectrosc. Relat. Phenom.* **1994**, *67*, 529−622.

(47) Ghiasi, M.; Delgado-Jaime, M. U.; Malekzadeh, A.; Wang, R.-P.; Miedema, P. S.; Beye, M.; De Groot, F. M. F. Mn and Co Charge and Spin Evolutions in LaMn1-XCoxO3 Nanoparticles. *J. Phys. Chem. C* **2016**, *120*, 8167−8174.

(48) Abbate, M.; De Groot, F. M. F.; Fuggle, J. C.; Fujimori, A.; Strebel, O.; Lopez, F.; Domke, M.; Kaindl, G.; Sawatzky, G. A.; Takano, M.; Takeda, Y.; Eisaki, H.; Uchida, S.; Uchida, S. Controlled-valence properties ofLa1−xSrxFeO3andLa1−xSrxMnO3studied by soft-x-ray absorption spectroscopy. *Phys. Rev. B: Condens. Matter Mater. Phys.* **1992**, *46*, 4511−4519.

(49) Castleton, C. W. M.; Altarelli, M. Orbital ordering in the manganites: Resonant x-ray scattering predictions at the manganese-LIIandLIIIedges. *Phys. Rev. B: Condens. Matter Mater. Phys.* **2000**, *62*, 1033−1038.

(50) Zimmermann, P.; Bouldi, N.; Hunault, M. O. J. Y.; Sikora, M.; Ablett, J. M.; Rueff, J.-P.; Lebert, B.; Sainctavit, P.; de Groot, F. M. F.; Juhin, A. 1s2p Resonant Inelastic X-Ray Scattering Magnetic Circular Dichroism as a Probe for the Local and Non-Local Orbitals in CrO2. *J. Electron Spectrosc. Relat. Phenom.* **2018**, *222*, 74−87.

(51) Lakshmi, S.; Endo, T.; Reddy, G. S. Electronic (Absorption) Spectra of 3d Transition Metal Complexes. *Adv. Aspects Spectrosc.* **2012**, 1−48.

(52) Valencia, S.; Gaupp, A.; Gudat, W.; Abad, L.; Balcells, L.; Martínez, B. Impact of microstructure on the Mn valence of La2/3Ca1/3MnO3 thin films. *Phys. Rev. B: Condens. Matter Mater. Phys.* **2007**, *75*, 184431.

(53) Mierwaldt, D.; Mildner, S.; Arrigo, R.; Knop-Gericke, A.; Franke, E.; Blumenstein, A.; Hoffmann, J.; Jooss, C. In Situ XANES/XPS Investigation of Doped Manganese Perovskite Catalysts. *Catalysts* **2014**, *4*, 129−145.

(54) Schmid, H. K.; Mader, W. Oxidation States of Mn and Fe in Various Compound Oxide Systems. *Micron* **2006**, *37*, 426−432.

(55) Hemberger, J.; Krimmel, A.; Kurz, T.; Krug von Nidda, H.-A.; Ivanov, V. Y.; Mukhin, A. A.; Balbashov, A. M.; Loidl, A. Structural, Magnetic, and Electrical Properties of Single-Crystalline La1-XSrxMnO3 (0.4<x<0.85). *Phys. Rev. B: Condens. Matter Mater. Phys.* **2002**, *66*, 094410.